YALE
PEABODY
MUSEUM

P.O. BOX 208118 | NEW HAVEN CT 06520-8118 USA | PEABODY.YALE. EDU

JOURNAL OF MARINE RESEARCH

The *Journal of Marine Research,* one of the oldest journals in American marine science, published important peer-reviewed original research on a broad array of topics in physical, biological, and chemical oceanography vital to the academic oceanographic community in the long and rich tradition of the Sears Foundation for Marine Research at Yale University.

An archive of all issues from 1937 to 2021 (Volume 1–79) are available through EliScholar, a digital platform for scholarly publishing provided by Yale University Library at https://elischolar.library.yale.edu/.

Requests for permission to clear rights for use of this content should be directed to the authors, their estates, or other representatives. The *Journal of Marine Research* has no contact information beyond the affiliations listed in the published articles. We ask that you provide attribution to the *Journal of Marine Research*.

Yale University provides access to these materials for educational and research purposes only. Copyright or other proprietary rights to content contained in this document may be held by individuals or entities other than, or in addition to, Yale University. You are solely responsible for determining the ownership of the copyright, and for obtaining permission for your intended use. Yale University makes no warranty that your distribution, reproduction, or other use of these materials will not infringe the rights of third parties.

This work is licensed under a Creative Commons Attribution-NonCommercial-ShareAlike 4.0 International License.
https://creativecommons.org/licenses/by-nc-sa/4.0/

Journal of Marine Research, 51, 273–292, 1993

The stability of an axially symmetric warm-core model eddy on a stratified ocean

by John Kroll[1]

ABSTRACT

The linear stability of an axially symmetric model of a warm-core eddy over a stratified ocean of infinite depth is investigated using asymptotic techniques for large wavenumber and small Burger number. The development is similar to previous work on the stability of a geostrophic front (Kroll, 1992) and the results found there can be modified and applied to most oceanic eddies. The most important result is that instability occurs in a region confined at the edge of the eddy with maximum width of a fraction of the radius given approximately by the Rossby number for realistic eddies. We expect the instability to produce turbulence and contribute to the breakdown of the interface between the eddy and the surrounding ocean in this region.

1. Introduction

Warm-core, anticyclonic eddies have been observed extensively in the ocean (Joyce, 1984; Joyce *et al.,* 1984). The largest of these has been observed to range up to 300 km in diameter off the northern part of the Gulf stream and up to 370 km in the Gulf of Mexico. The Rossby number, ϵ, the ratio of the average angular swirl speed to the Coriolis frequency, is a measure of the importance of the nonlinear terms in the equations of motion describing an eddy. For these large warm-core eddies, ϵ ranges up to $\frac{1}{4}$.

Cold-core, cyclonic eddies of comparable diameter and values of ϵ also exist. Richardson (1980) observed one for $\epsilon \approx \frac{3}{8}$. There are also somewhat smaller warm-core, anticyclonic vortices with diameters less than 100 km and with comparable values of ϵ which have been called submesoscale coherent vortices (SCV) by McWilliams (1985). Armi *et al.* (1989) observed an SCV over its entire lifetime of two years. This eddy had an initial diameter of about 50 km and ϵ around $\frac{1}{3}$.

For ϵ sufficiently small, one can use the quasi-geostrophic approximation to model an eddy. However, the values of ϵ noted above are not sufficiently small. For ϵ of order one, the 'reduced gravity' or '1.5 layer' model has been used fruitfully by Cushman-Roisin *et al.* (1985) to model the dynamics of eddies. This model consists of

1. Department of Mathematical Science and the Center for Coastal Physical Oceanography, Old Dominion University, Norfolk, Virginia, 23529, U.S.A.

an active homogeneous layer of inviscid fluid over an inactive homogeneous layer of higher density and infinite depth. The aspect ratio of the depth to the horizontal scale in the top layer is assumed small with time derivative and nonlinear terms of order one.

A logical extension is to add stratification to the lower layer. This will allow energy to be propagated away from the eddy in the form of internal waves. Thus we will investigate the stability of an axially symmetric, warm-core, anticyclonic model eddy over an infinitely deep, linearly stratified ocean.

This investigation is a direct continuation of previous work (Kroll, 1992). There the stability of a geostrophic front with constant slope over a stratified ocean was investigated using asymptotic methods for large horizontal wavenumber and relatively weak stratification. The front was called canonical because it should approximate more complicated flows. It will be shown that it indeed approximates the stability of a model eddy. This canonical front problem, which will henceforth be referred to as (F), is reviewed first.

The flow is unstable for wave perturbations in the direction of the mean flow with wavenumbers along the front larger than f/V_0, where V_0 is the speed of the mean flow, becoming more unstable with increasing wavenumber. The region of instability, however, is essentially limited to a relatively small portion of the front at the vertex where the frontal interface meets the surface. This region has a maximum horizontal extent given approximately by V_0/f, and the region becomes smaller with increasing wavenumber. We would expect this region to become turbulent and generate internal waves that propagate into the interior. However, if the front is viewed as the edge of an eddy or boundary current, we would conclude that these flows are essentially stable since the instability is confined to such a small portion of the mean flow, typically less than 10 km versus a scale of 100 km.

The nature of the instability resembles that of the mixed layer model previously investigated by Kroll (1982, 1988). The unstable perturbations grow from energy from the mean flow. An increase in stratification, which increases the energy radiated away from the current, is actually destabilizing. This was first discussed for the nonrotating case by Ostrovskiy and Tsimring (1981) who pointed out that it is not a classical Kelvin-Helmholtz instability since the instability disappears with no stratification. They explain the nature of this instability using the concept of negative energy which was developed by Cairns (1979). In the classification scheme of Benjamin (1963) this is a class C instability, which is a Kelvin-Helmholtz type (but definitely not the classical Kelvin-Helmholtz).

2. Formulation of model

The development will parallel that of (F) using cylindrical rather than Cartesian coordinates. Figure 1 shows an axially symmetric eddy of homogeneous fluid with density ρ_1, surrounded by a continuously stratified ocean of infinite depth with

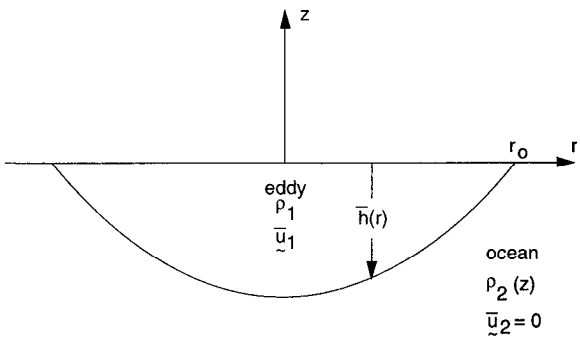

Figure 1. An axially symmetric warm-core eddy on a stratified ocean.

density $\rho_2(z)$, where $\rho_1 < \rho_2(z)$ everywhere. The eddy has a maximum radius, r_0, and maximum azimuthal speed, V_0, occurring at r_0. The flow regime in the eddy will be designated as the "eddy" and that in the stratified ocean as the "ocean." As in (F), we make the usual assumptions: hydrostatic balance, Bousinesq approximation in the ocean, a rigid lid at the surface, and the Coriolis parameter, f, constant.

The dimensionless equations of motion are for the eddy:

$$u_{1t} + u_1 u_{1r} - \frac{v_1^2}{r} + \frac{v_1 u_{1\theta}}{r} - v_1 = -(P_1 + h)_r \tag{1a}$$

$$v_{1t} + u_1 v_{1r} + \frac{u_1 v_1}{r} + \frac{v_1 v_{1\theta}}{r} + u_1 = -\frac{(P_1 + h)_\theta}{r} \tag{1b}$$

$$h_t + \frac{1}{r}[(rhu_1)_r + (hv_1)_\theta] = 0 \tag{1c}$$

and for the ocean:

$$u_{2t} - v_2 = -P_{2r} \tag{2a}$$

$$v_{2t} + u_2 = -\frac{P_{2\theta}}{r} \tag{2b}$$

$$P_{2zt} = -B^2 w_2 \tag{2c}$$

$$\frac{1}{r}[(ru_2)_r + v_{2\theta}] + w_{2z} = 0 \tag{2d}$$

with boundary conditions at $z = -h(r, \theta, t)$

$$h_t + u_2 h_r + \frac{v_2 h_\theta}{r} = -w_{2z}, \qquad h > 0 \tag{3a}$$

$$w_2 = 0, \qquad h = 0 \tag{3b}$$

and $$P_1 = P_2. \tag{3c}$$

As in (F), the quantities $P_{1,2}$ represent in dimensional terms $p_{1,2} - g\Delta\rho h$ where p is the actual pressure.

The nondimensionalization is as follows, similar to (F): $(u, v) \sim V_0, r \sim L = V_0/f$, $(h, z) \sim H = V_0^2/g', w \sim Hf, t \sim 1/f, P \sim \rho_0 f L V_0$, where $g' = g\Delta\rho/\rho_0, B = HN/Lf$ and $N^2 = -g\rho'_2(z)/\rho_0$ (the square of the Brunt-Vaisälä frequency). The choice for the length scale L is based on results from (F). As before ρ_0 is the reference density for the ocean, $\rho'_2(z)$ is the density gradient which is negative and assumed constant, and $\Delta\rho = \rho_0 - \rho_1$. We assume $|\rho'_2 h/\Delta\rho| \ll 1$ which implies that $B^2 \ll 1$. In essence we are assuming that the density difference in the stratified ocean in the interval over the eddy depth is much smaller than the density difference between the eddy and the ocean.

For the steady state we assume that all t and θ derivatives vanish and $u_2 = v_2 = 0$, so $P_1 = P_2 = 0$. For simplicity suppose the radial velocity, u, in the eddy to be zero and the azimuthal velocity, v, to vary linearly with r (solid body rotation); then the shape of the eddy is parabolic. Thus for the steady state

$$\bar{v}_1 = -\epsilon r, \tag{4a}$$

$$\bar{h} = \frac{1}{2}\epsilon(1 - \epsilon)(\bar{r}^2 - r^2) \tag{4b}$$

an axially symmetric eddy where the Rossby number, $\epsilon = V_0/fr_0$, is $1/\bar{r}$ and $\bar{r} = r_0/L$ is the value of dimensionless r at dimensional $r = r_0$. For a physically realizable warm-core eddy, ϵ must be such that $0 < \epsilon < 1$. This simple model eddy has a uniform angular speed, Ω, which has been observed approximately in nature (e.g. Armi *et al.* (1989) where $\Omega \approx f/3$).

The perturbation equations are found by expressing the dependent variable in steady and perturbation parts, $(\ ) = (\bar{\ }) + (\ )'$. From (1) we obtain for the eddy, dropping the primes:

$$u_{1t} - \frac{2\bar{v}_1 v_1}{r} + \frac{\bar{v}_1 v_{1\theta}}{r} - v_1 = -(P_1 + h)_r \tag{5a}$$

$$v_{1t} + \bar{v}_{1r} u_1 + \frac{\bar{v}_1 u_1}{r} + \frac{\bar{v}_1 v_{1\theta}}{r} + u_1 = -\frac{(P_1 + h)_\theta}{r} \tag{5b}$$

$$h_t + \frac{1}{r}[r\bar{h}_r u_1 + \bar{h}(ru_1)_r + \bar{h}v_{1\theta}] = 0. \tag{5c}$$

The perturbation equations for the ocean still have the form (2). The boundary

conditions (3) at $z = -\bar{h}(r)$ becomes

$$h_t + \bar{h}_r u_2 = -w_2, \qquad \bar{h} > 0 \tag{6a}$$

$$0 = w_2, \qquad \bar{h} = 0. \tag{6b}$$

For the linear stability analysis, we assume a wave solution in θ:

$$(\ ) = (\hat{\ })(r)e^{-i(m\theta+\omega t)} \tag{7}$$

where the angular mode number, m, is an integer which will turn out to be positive for unstable waves. Then eliminating u_1 and v_1 in (5) we obtain for the eddy:

$$r^2(\bar{r}^2 - r^2)\hat{h}_{rr} + r(\bar{r}^2 - 3r^2)\hat{h}_r + (\lambda^2 r^2 - \bar{r}^2 m^2)\hat{h}$$
$$= -\left\{r^2(\bar{r}^2 - r^2)\hat{P}_{1rr} + r(\bar{r}^2 - 3r^2)\hat{P}_{1r} + \left[\left(\frac{-2m\tilde{f}}{\tilde{\omega}} + m^2\right)r^2 - \bar{r}^2 m^2\right]\hat{P}_1\right\} \tag{8}$$

where $\lambda^2 = -2m\tilde{f}/\tilde{\omega} + m^2 + 2(\tilde{\omega}^2 - \tilde{f}^2)/[\epsilon(1-\epsilon)]$, $\tilde{f} = 1 - 2\epsilon$, and $\tilde{\omega} = \omega - \epsilon m$.

Eliminating all but $\hat{P}_2$ in (2), we obtain for the ocean:

$$\nu^2\hat{P}_{2zz} - \hat{P}_{2rr} - \frac{\hat{P}_{2r}}{r} + \frac{m^2\hat{P}_2}{r^2} = 0 \tag{9}$$

where $\nu^2 = (\omega^2 - 1)/B^2$. The boundary conditions at $z = -\bar{h}(r)$ are

$$\nu^2 B^2\hat{h} = \nu^2\hat{P}_{2z} - \bar{h}_r\left(\hat{P}_{2r} + \frac{m\hat{P}_2}{\omega r}\right), \qquad \bar{h} > 0 \tag{10a}$$

$$\hat{w}_2 = 0, \qquad \bar{h} = 0 \tag{10b}$$

and

$$\hat{P}_1 = \hat{P}_2. \tag{10c}$$

There is also the radiation condition that no energy may come from $|(r, z)| \to \infty$.

Eqs. (8) and (9), together with the interface conditions (10) and the radiation condition, constitute the system to be solved.

3. Special case: no stratification

For no stratification in the ocean ($B = 0$), we have $P_2 = P_1 = 0$. Letting $R = r/\bar{r}$, Eq. (8) becomes

$$R^2(1 - R^2)\hat{h}_{RR} + (R - 3R^3)\hat{h}_R + (R^2\lambda^2 - m^2)\hat{h} = 0, \tag{11}$$

with the boundary conditions that $\hat{h}$ be bounded at $R = 0$ and $R = 1$. Cushman-Roisin (1986) and Ripa (1987) have shown that we are to expect eigenfunctions involving finite degree polynomials. If we write $\hat{h} = \Sigma_{n=0}^{\infty} a_n R^{n+c}$ and use the method of

Frobenius, we find $c = |m|$ and

$$\lambda^2 = (2n + |m|)(2n + 2 + |m|). \tag{12}$$

The odd coefficients vanish and the eigenfunctions can be shown to be given by

$$\hat{h}_N = R^{|m|} \sum_{n=0}^{N} b_n(N) R^{2n}, \tag{13a}$$

$$\text{where } b_{n+1}(N) = -\frac{(N-n)(N+n+1+|m|)}{(n+1)(n+1+|m|)} b_n(N) \tag{13b}$$

is the recursion relation. The first three eigenvalues and eigenfunctions are:

$$\lambda_0^2 = |m|(|m| + 2), \qquad \hat{h}_0 = R^{|m|}$$

$$\lambda_1^2 = (|m| + 2)(|m| + 4), \hat{h}_1 = \left(1 - \frac{2 + |m|}{1 + |m|} R^2\right) R^{|m|}$$

$$\lambda_2^2 = (|m| + 4)(|m| + 6), \hat{h}_2 = \left(1 - \frac{2(3 + |m|)}{1 + |m|} R^2 + \frac{(4 + |m|)(3 + |m|)}{(2 + |m|)(1 + |m|)} R^4\right) R^{|m|}$$

We want to examine the eigenfrequency, ω. Rewriting (12), using the definition of λ^2,

$$\tilde{\omega}^3 - (\tilde{f}^2 + Q)\tilde{\omega} - m\bar{\epsilon}\tilde{f} = 0 \tag{14}$$

where $Q = \bar{\epsilon}[2n(n + 1) + |m|(2n + 1)]$, $\bar{\epsilon} = \epsilon(1 - \epsilon)$, $\tilde{\omega} = \omega - \epsilon m$, and $\tilde{f} = 1 - 2\epsilon$. Analogous to the results in (F), the discriminant $D = m^2\bar{\epsilon}^2\tilde{f}^2/4 - (\tilde{f}^2 + Q)^3/27$ is always < 0 except for $n = 0$ when $D = 0$ at one value of ϵ for each value of $m = 0, \pm 1, \pm 2, \ldots$. Hence the system is always neutrally stable as found by Ripa (1987). Because of the $R^{|m|}$ variation, the magnitude of the eigenfunctions for $m \neq 0$ are most significant toward $R = 1$, the edge of the eddy, analogous to the result in (F).

We noted in (F) that for the $B = 0$ case the front becomes unstable if a bottom is added. Interestingly, Ripa (1992) has shown that this model eddy is also unstable for the $B = 0$ case if a bottom is added.

4. Asymptotic solution for stratified ocean ($B > 0$)

We follow a procedure similar to that in (F). We find an asymptotic solution for large $|m|$ in the ocean using ray theory. We then use this result, evaluated at the interface, to find an asymptotic solution in the eddy away from both the boundary, $R = 1$, and a turning point at $R = |m/\lambda| = |\gamma|$. It is then necessary to find boundary layer solutions near $R = 1$ and $R = |\gamma|$. Finally, all the solutions are matched to lowest order to give an approximate eigenvalue equation for ω.

a. Rays in the ocean. Though exact solutions to (9) are available in the form of Bessel functions, these would not be useful in connecting with the eddy. Thus we use the approximate ray theory method. We assume a solution to (9) in the form

$$\hat{P} = A(r, z)e^{i|m|S(r,z)} \tag{15}$$

which yields

$$\begin{aligned} \nu^2(A_{zz} + 2i|m|S_zA_z + i|m|S_{zz}A - m^2S_z^2A) \\ - (A_{rr} + 2i|m|S_rA_r + i|m|S_{rr}A - m^2A) \\ - \frac{1}{r}(A_r + i|m|S_rA) + \frac{m^2A}{r^2} = 0. \end{aligned} \tag{16}$$

We then assume $A = A_0 + 1/|m|A_1 + \ldots$ with $|m|$ large. To lowest order in $1/|m|$ the eiconal equation is

$$F(r, z, p, q) = -\nu^2q^2 + p^2 + \frac{1}{r^2} = 0 \tag{17}$$

where $p = S_r$ and $q = S_z$ are wavenumbers in r and z respectively.

As in (F), we use characteristics to solve (17) which are derived from the solutions of the set of differential equations:

$$\frac{dr}{ds} = F_p, \qquad \frac{dz}{ds} = F_q$$

$$\frac{dp}{ds} = -F_r, \qquad \frac{dq}{ds} = -F_z$$

and

$$\frac{dS}{ds} = pF_p + qF_q.$$

On the interface, $z = -\bar{h}(r)$, we define $s = 0$ and $z = -\bar{h}(\tau)$ where s and τ are the ray variables with τ being r on the interface. We then find that $q = \bar{q}(\tau)$ is constant on a ray and p is given by $p^2 = \bar{p}^2 + [(1/\tau^2) - (1/r^2)]$, where $\bar{q}$ and $\bar{p}$ are evaluations of q and p at the interface. The parametric equations for the rays are:

$$z = -2\nu^2\bar{q}s - \bar{h}(\tau) \tag{18a}$$

$$r^2 = \frac{\left[2\left(\bar{p}^2 + \frac{1}{\tau^2}\right)s + \bar{p}\tau\right]^2 + 1}{\bar{p}^2 + \frac{1}{\tau^2}}. \tag{18b}$$

Continuing to follow (F), we use the strip condition at $s = 0$ that

$$\frac{dS}{d\tau} = p\left(\frac{dr}{d\tau}\right) + q\left(\frac{dz}{d\tau}\right)$$

with (17) to find $\bar{p}$ and $\bar{q}$ in terms of $\bar{S}'(\tau) \equiv (d\bar{S}/d\tau)$, where $\bar{S}(\tau)$ is the value of S at the interface:

$$\bar{q}(\tau) = \frac{-\bar{\epsilon}\tau\bar{S}' + \sqrt{\nu^2\bar{S}'^2 + \nu^2/\tau^2 - \bar{\epsilon}^2}}{\nu^2 - \bar{\epsilon}^2\tau^2} \tag{19a}$$

$$\bar{p}(\tau) = \frac{\nu^2\bar{S}' - \bar{\epsilon}\tau\sqrt{\nu^2\bar{S}'^2 + \nu^2/\tau^2 - \bar{\epsilon}^2}}{\nu^2 - \bar{\epsilon}^2\tau^2} \tag{19b}$$

where $\bar{\epsilon} = \epsilon(1 - \epsilon)$. We again use the fact that the normal component of the group velocity at the interface must be directed into the ocean to determine the proper signs in front of the radicals. This normal component is proportional to $\langle -\bar{h}'(r), -1\rangle \cdot \langle (dr/ds),(dz/ds)\rangle$ which equals $\frac{1}{2}\sqrt{\nu^2\bar{S}'^2 + \nu^2/\tau^2 - \bar{\epsilon}^2}$ for the proper sign. Also we can find $S(s, \tau)$ from the set of differential equations for the characteristics:

$$S(s, \tau) = \bar{S}(\tau) + \tan^{-1}(\bar{p}\tau) - \tan^{-1}(2\nu^2\bar{q}^2 s + \bar{p}\tau). \tag{20}$$

The elimination of s between the equations of (18) reveals that the ray paths are hyperbolas. These paths are actually the generating curves of surfaces of revolution about the z-axis and represent the energy flux for the internal waves. Figure 2 shows schematically some of these paths. We can show that for r large the rays near the edge of the eddy ($r \to \bar{r}$) are approximated by the straight line paths of (F). All the rays that are directed toward $r = 0$ turn at a point where the radial group speed vanishes before reaching $r = 0$, the center of the eddy. Figure 2 does not represent a typical ray field but only different possible ray configurations. The dashed-line extensions illustrate the hyperbolic shape and are not rays since there are of course no rays in the eddy.

From the next order from (16), we have

$$\frac{dA_0}{ds} - \left(\nu^2 S_{zz} - S_{rr} - \frac{S_r}{r}\right)A_0 = 0. \tag{21}$$

Using (18) to calculate $\partial/\partial z\, \tau(r, z)$ and $\partial/\partial r\, \tau(r, z)$, we can then use (19) to find $S_{zz} = \bar{q}_z = \bar{q}_\tau\, (\partial/\partial z)\tau$ and $S_{rr} = \bar{p}_r = \bar{p}_\tau(\partial/\partial r)\tau$ in terms of s and show that

$$A_0(s, \tau) = G(\tau)[E(\tau)(2\nu^2\bar{q}^2 s + \bar{p}\tau) - \bar{q}'(\tau)]^{-1/2} \tag{22}$$

where $E(\tau) = \bar{q}[(\tau\bar{S}')' - (\tau\bar{q})'] - \bar{q}'\bar{p}\tau$ and $G(\tau)$ an arbitrary function.

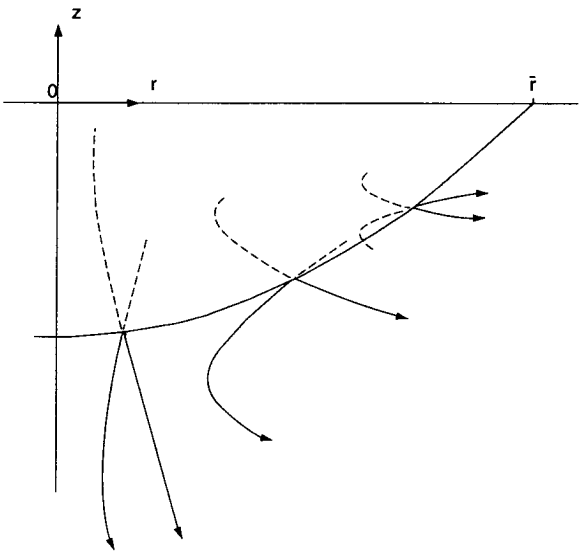

Figure 2. Possible hyperbolic ray paths into the ocean. The dashed extensions are not rays, but are shown to illustrate the hyperbolic shape of each ray.

b. Asymptotic solution in the eddy. From (8) we can show

$$H''(R) + \left(\frac{\lambda^2 R^2 - m^2}{\tilde{h}R^2} + \frac{1}{4R^2} + \frac{2 - R^2}{\tilde{h}^2}\right)H(R) = -\left\{\tilde{P}''(R) + \left[\frac{-2m\tilde{f}}{\tilde{\omega}\tilde{h}} - \frac{m^2}{4R^2} + \frac{1}{4R^2} + \frac{2 - R^2}{\tilde{h}^2}\right]\tilde{P}(R)\right\} \tag{23}$$

where $R = r/\bar{r}$, $H = \hat{h}\sqrt{R\tilde{h}}$, $\tilde{P} = \hat{P}\sqrt{R\tilde{h}}$, and $\tilde{h} = 1 - R^2$. For m and λ large, there will be a turning point for the left side of (23) in R where $\lambda^2 R^2 - m^2$ vanishes. Assuming λ real and for $|m/\lambda| < R < 1$ but R not near the end points, we look for an oscillatory solution. So we assume

$$H = \tilde{H}(R)e^{i|m|\tilde{S}(R)} \tag{24}$$

where $\tilde{H} = \tilde{H}_0 + 1/|m|\,\tilde{H}_1 + \ldots$ and $\tilde{S}(R) = \bar{S}(r)$.

For $\hat{P}_2 = A_0 e^{i|m|S(r,z)}$, the interface condition (10) then yields to lowest order for $s = 0$ (where $r = \tau$)

$$A_0(0, \tau) = \frac{(\omega^2 - 1)\sqrt{\bar{r}}\tilde{H}_0}{i|m|\sqrt{\tau\tilde{h}}\left[D_0 - \dfrac{i\epsilon m}{\omega|m|}\right]} \tag{25}$$

where $D_0 = \sqrt{\nu^2\bar{S}'^2 - \bar{\epsilon}^2 + \nu^2/\tau^2}$ and $S(r, z) = S(\tau, -\bar{h}(\tau)) = \bar{S}(\tau)$. Using (25) in (22),

we can find $G(\tau)$, but we do not need it to calculate the eigenvalue to lowest order. When the radical in (22) vanishes a caustic appears in the wave field.

We note that from (25) $\tilde{P} = O(1/|m|)\tilde{H}$. So letting $\tilde{P} = (1/|m|)[\tilde{P}_0 + (1/|m|)\tilde{P}_1 + \ldots]e^{i|m|\tilde{S}(R)}$ and using (24) in (23), we can show to lowest order

$$\tilde{S}'(R) = \bar{r}\bar{S}'(r) = \pm\,\bar{\sigma}'(R) = \pm\sqrt{\frac{R^2-\gamma^2}{\gamma^2R^2\tilde{h}}} \tag{26}$$

where $\gamma = m/\lambda$.

For the next order we have

$$2i\tilde{S}'(R)\tilde{H}_0'(R) + i\tilde{S}''(R)\tilde{H}_0(R) = \left(\tilde{S}'(R)^2 + \frac{1}{R^2}\right)\tilde{P}_0(R)$$

and, using the fact that $A_0 = (1/|m|)\tilde{P}_0/\sqrt{R\tilde{h}}$ and (25), we connect the rays with the eddy and obtain

$$\tilde{H}'_0 + \left[\frac{\tilde{S}''}{2\tilde{S}'} + \frac{(\omega^2-1)\left(\tilde{S}'^2 + \dfrac{1}{R^2}\right)}{2\tilde{S}'\left(D_0 - \dfrac{i\bar{\epsilon}m}{\omega|m|}\right)}\right]\tilde{H}_0 = 0. \tag{27}$$

The solution can be written as

$$\tilde{H}_0(R) = \frac{C}{\sqrt{\tilde{S}'(R)}}e^{-(1/2)sn(\omega^2-1)\bar{I}(R)} \tag{28}$$

where sn is the sign in (26), C is an arbitrary constant and

$$\bar{I}(R) = \frac{1}{\gamma^2}\int_1^R \frac{\dfrac{1-\gamma^2}{1-t^2}}{\sqrt{\dfrac{t^2-\gamma^2}{\gamma^2t(1-t^2)}}\left[\sqrt{\dfrac{\nu^2(1-\gamma^2)}{\gamma^2\bar{r}^2(1-t^2)} - \bar{\epsilon}^2} - \dfrac{i\bar{\epsilon}m}{\omega|m|}\right]}dt \tag{29}$$

using the fact that we can show $D_0 = \sqrt{\nu^2(1-\gamma^2)/\gamma^2\bar{r}^2(1-R^2) - \bar{\epsilon}^2}$.

If we make the change of variable $t^2 = 1 - 2y/\bar{r}$, we can show that the integral (29) can be written in the form:

$$\bar{I}(R) = -\frac{\beta\bar{y}_c\omega^2}{\omega^2-1}\left\{\int_0^{\bar{y}(R)}\frac{\sqrt{\bar{\nu}^2\bar{y}_c - y}}{\sqrt{\bar{y}_c - y}(\bar{y}_p - y)}dy + \frac{im}{\omega|m|}\int_0^{\bar{y}(R)}\frac{\sqrt{y}}{\sqrt{\bar{y}_c - y}(\bar{y}_p - y)}dy\right\} \tag{30}$$

where $\beta = 1/[\gamma(1-\epsilon)]$, $\bar{y}_c = (1/2)\bar{r}(1-\gamma^2)$, $\bar{y}_p = \omega^2\beta^2\bar{y}_c/B^2$, $\bar{\nu}^2 = \nu^2\beta^2$, and $\bar{y} = (1/2)\bar{r}(1-R^2)$. The integrals here are the same form as those of Eq. (43) in (F). So we can use the results there, including the analytic continuation properties, to evaluate

(30). Thus, using $\bar{y}$ as the independent variable so that $\bar{I}(R) = I(\bar{y})$, (30) becomes:

$$I(\bar{y}) = -\frac{\beta\bar{y}_c\omega^2}{\omega^2-1}\left\{\log\frac{(\chi-1)(\bar{\nu}+1)}{(\chi+1)(\bar{\nu}-1)} - \chi_0\log\frac{(\chi-\chi_0)(\bar{\nu}+\chi_0)}{(\chi+\chi_0)(\bar{\nu}-\chi_0)} - \frac{2im}{\omega|m|}\left(\tan^{-1}\psi - \psi_0\tan^{-1}\frac{\psi}{\psi_0}\right)\right\} \tag{31}$$

where $\chi^2 = (\bar{\nu}^2\bar{y}_c - \bar{y})/(\bar{y}_c - \bar{y})$, $\chi_0^2 = (\bar{y}_p - \bar{\nu}^2\bar{y}_c)/(\bar{y}_p - \bar{y}_c) = \beta^2/(\omega^2\beta^2 - B^2)$, $\psi^2 = \bar{y}/(\bar{y}_c - \bar{y})$, and $\psi_0^2 = \bar{y}_p/(\bar{y}_p - \bar{y}_c)$, with cuts for the functions down the negative imaginary axis as in (F). We can again show that (31) can be used for the case where $\bar{y} > \bar{y}_p$ when a singularity occurs on the path of integration at $\bar{y} = \bar{y}_p$.

So to lowest order for $|m/\lambda| < R < 1$, we have

$$\hat{h}_0 = \frac{1}{\sqrt{R(1-R^2)\bar{\sigma}'}}e^{-1/2(\omega^2-1)I}\{C_1e^{i|m|\bar{\sigma}} + C_2e^{-i|m|\bar{\sigma}}\} \tag{32}$$

where from (26),

$$\bar{\sigma}(R) = \int_1^R \sqrt{\frac{t^2-\gamma^2}{\gamma^2(1-t^2)}}\frac{dt}{t} = \frac{1}{\gamma}\left[\tan^{-1}\sqrt{\frac{R^2-\gamma^2}{1-R^2}} - \frac{\pi}{2}\right] - \left[\tan^{-1}\sqrt{\frac{R^2-\gamma^2}{\gamma^2(1-R^2)}} - \frac{\pi}{2}\right]$$

c. Expansions about special points. Analogous to (F), (23) is singular at $R = 1$. If we let $1 - R = (1/m^2)\xi$, to lowest order we have

$$H_{0\xi\xi} + \left(\frac{1-\gamma^2}{2\gamma^2\xi} + \frac{1}{4\xi^2}\right)H_0 = 0,$$

which has the solution bounded at $R = 1$:

$$\hat{h}_0 = \frac{H_0}{\sqrt{R(1-R^2)}} = \frac{D_1\sqrt{\xi}}{\sqrt{R(1-R^2)}}J_0\left(\sqrt{2\frac{1-\gamma^2}{\gamma^2}\xi}\right) \tag{33}$$

where J_0 is a Bessel function.

Also analogous to (F), we have a turning point at $R = m/\lambda = \gamma$. If we let $R - \gamma = |m|^{-2/3}\zeta$, to lowest order we have

$$H_{0\zeta\zeta} + \frac{2\zeta}{\gamma^3(1-\gamma^2)}H_0 = 0$$

which has a solution which decays for $\zeta \to -\infty$:

$$\hat{h}_0 = \frac{H_0}{\sqrt{R(1-R^2)}} = \frac{B_0}{\sqrt{R(1-R^2)}}Ai\left[-\left(\frac{2}{\gamma^3(1-\gamma^2)}\right)^{1/3}\zeta\right] \tag{34}$$

where Ai is an Airy function.

d. Matching solutions. We must match (33) for ξ large with (32) for $R \to 1$ (or $\bar{y} \to 0$). Using the asymptotic properties of the functions involved, we find the common part:

$$\hat{h}_0 = \frac{D_1\sqrt{\gamma|m|}}{\sqrt{2\pi(1-\gamma^2)}(1-R)^{1/4}} \cos\left(\sqrt{2\frac{1-\gamma^2}{\gamma^2}}\,\xi - \frac{\pi}{4}\right) \tag{35a}$$

and the matching conditions for the constants:

$$\frac{D_1\sqrt{\gamma|m|}}{2\sqrt{2\pi(1-\gamma^2)}} e^{i(\pi/4)} = \frac{C_1}{[2(1-\gamma^2)]^{1/4}}, \quad \frac{D_1\sqrt{\gamma|m|}}{2\sqrt{2\pi(1-\gamma^2)}} e^{-i(\pi/4)} = \frac{C_2}{[2(1-\gamma^2)]^{1/4}} \tag{35b}$$

Likewise, we must match (34) for ζ large with (32) for $R \to \gamma$ ($\bar{y} \to \bar{y}_c$). We can find the common part:

$$\hat{h}_0 = \frac{B_0\left[\frac{1}{2}\gamma^3(1-\gamma^2)\right]^{1/12}}{\sqrt{\gamma(1-\gamma^2)\pi}\zeta^{1/4}} \sin\left[\frac{2}{3}\sqrt{\frac{2}{\gamma^3(1-\gamma^2)}}\,\zeta^{3/2} + \frac{\pi}{4}\right] \tag{36a}$$

and the matching conditions for the constants:

$$\begin{aligned}
\left[\frac{\gamma}{2}(1-\gamma^2)\right]^{1/4} C_1 e^{-[(\omega^2-1)/2]I(\bar{y}_c)-i(\pi/2)\lambda(1-\gamma)} &= \frac{B_0[\gamma(1-\gamma^2)]^{1/12}\, e^{i(\pi/4)}}{\sqrt{\pi}2^{4/3}|m|^{1/6}i}, \\
\left[\frac{\gamma}{2}(1-\gamma^2)\right]^{1/4} C_2 e^{[(\omega^2-1)/2]I(\bar{y}_c)+i(\pi/2)\lambda(1-\gamma)} &= -\frac{B_0[\gamma(1-\gamma^2)]^{1/12}\, e^{-i(\pi/4)}}{\sqrt{\pi}2^{4/3}|m|^{1/6}i}.
\end{aligned} \tag{36b}$$

Solving (35b) and (36b) simultaneously, we can show that

$$\frac{\pi}{2}(\lambda - |m|) - \frac{i}{2}(\omega^2 - 1)I(\bar{y}_c) = \frac{\pi}{2}(2n+1), \qquad n = 0, 1, 2, \ldots \tag{37}$$

gives the eigenvalues, λ. Using the definition of λ from (8), we then have the equation for the eigenfrequencies, ω. This result is very similar to that of (F) and can be shown to be identical in the limit as $\bar{r} = 1/\epsilon \to \infty$ if we identify m, the angular mode number, with $\bar{r}k$, where k is the dimensionless along the front wavenumber of (F). This is as it should be since the edge of this model eddy, as its radius is approaching infinity, is becoming a canonical front. This means that if the mean flow does not vary much and the mean depth approaches a linear shape near the edge of the eddy, then the shape and velocity distribution of the rest of the eddy are relatively unimportant.

For an unstratified ocean, where $B = 0$, Eq. (37) yields $\lambda^2 = (2n + 1 + |m|)^2$ in comparison to the exact value from (12) of $\lambda^2 = (2n + |m|)(2n + 2 + |m|)$. So unlike the canonical case the asymptotic result is not exact for $B = 0$. We can show that $(\lambda_a^2 - \lambda_e^2)/\lambda_e^2 = 1/\lambda_e^2$ where λ_e is exact (for $B = 0$) and λ_a approximate. We will

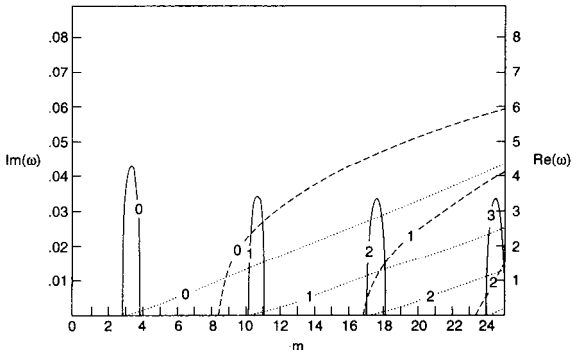

Figure 3. The real and imaginary parts of ω versus the angular mode number m for various small values for the radial mode number n and for $\epsilon = .25$ and $B = .1$. The solid curves are values of the growthrate, $Im(\omega)$, for subinertial values of the frequency, $Re(\omega)$. The dashed curves are values of $Im(\omega)$ for superinertial values of $Re(\omega)$. The dotted curves are values of $Re(\omega)$. The numbers on the curves are values of n.

see that since the values of $|m|$ are discrete the lowest value of $|m|$ that can be unstable is $|m| = 1$ so that we always have $1/\lambda^2 < 1/3$ which is not all that good. However the approximation improves quickly with increasing m and n.

It is observed from the results from (F) that the smallest possible value of the wavenumber, k, for instability occurs when ω and B are set to zero. If this is applied to (37), we find that for instability we must have

$$m > \frac{(1-\epsilon)(2n+1) + \sqrt{(2n+1)^2(1-\epsilon^2) - 4\epsilon(1-2\epsilon)}}{2\epsilon} \tag{38}$$

which reduces to $k > 2n + 1$, the result from (F), if we let $m \to (k/\epsilon)$ and $\epsilon \to 0$. As in (F), we will find that unstable waves all travel in the direction of the mean flow, i.e. $m > 0$.

The eigenfunctions associated with the eigenfrequencies will be quite similar to those from (F). These functions will be oscillatory in the interval, $\gamma < R < 1$, on the outer edge of the eddy as shown in (24), and will decay exponentially as $\exp\{-2/3\sqrt{[2/\gamma^3(1-\gamma^2)]}\,|m|\,|R-\gamma|^{3/2}\}$ in the interval $0 < R < \gamma$ as found from (34). Thus when there is instability the oscillations grow but the decaying portion remains relatively negligible by comparison, so that the instability is essentially confined to the outer edge. We expect the accuracy of our approximate eigenfunctions to be similar to those in (F) in balancing the energy equation. Thus we should have poor accuracy for $n = 0$, but rapid improvement for $n \geq 1$.

5. Results and discussion

Figure 3 shows the frequency, $Re(\omega)$, and the growthrate, $Im(\omega)$, versus the angular mode number m for fixed realistic value of ϵ and B. It is graphed as if m were

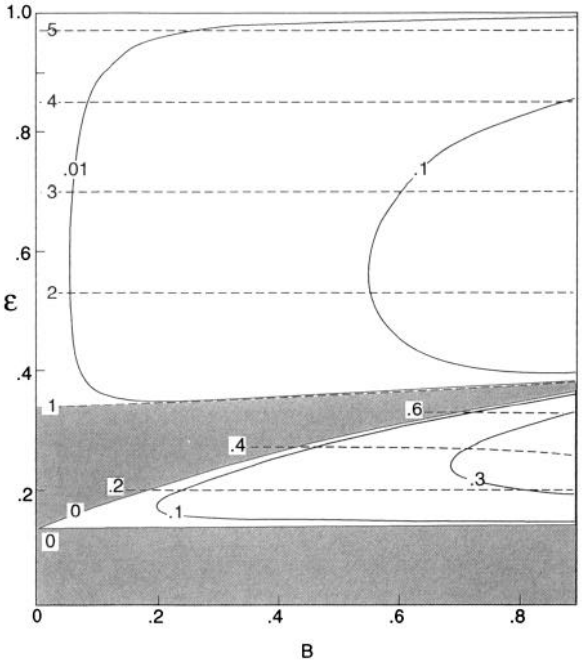

Figure 4. Contours of constant growthrate, $Im(\omega)$, (solid) and frequency, $Re(\omega)$, (dashed) in (B, ϵ) space for $n = 0$ and $m = 6$. The shaded region is neutrally stable.

continuous, but of course only integer values of m are applicable. For each radial mode n, we can clearly see the subinertial ($Re(\omega) < 1$) and the superinertial ($Re(\omega) > 1$) regimes as found in (F). Because m is an integer and the bandwidth on m is narrow for the subinertial regime, it is problematical whether there will be an integer within the band width and hence a subinertial instability. This bandwidth increases with B as can be seen on Figures 3, 4, and 5 in (F). Clearly there is no problem that there will be integer values for the superinertial regime. Thus superinertial waves would appear to dominate the instability.

Figures 4 and 5 show the level curves of constant frequency, $Re(\omega)$, and growthrate, $Im(\omega)$, in (B, ϵ) space. On Figure 4 can be clearly seen the superinertial and subinertial regions. For larger mode numbers m and n on Figure 5, we see that the subinertial region is becoming negligible. As B increases, the growthrate increases which exemplifies the type of instability discussed in the summary of (F) in the introduction.

In Figures 6, 7, 8, and 9 we show the level curves for the frequency, $Re(\omega)$, and the growthrate, $Im(\omega)$, in (n, m) space where only integer values of n and m are applicable. From these figures we see as in previous figures that the subinertial region is small compared to the superinertial region. For larger values of ϵ and smaller values of B, the subinertial region can be narrower than a line on the graph as

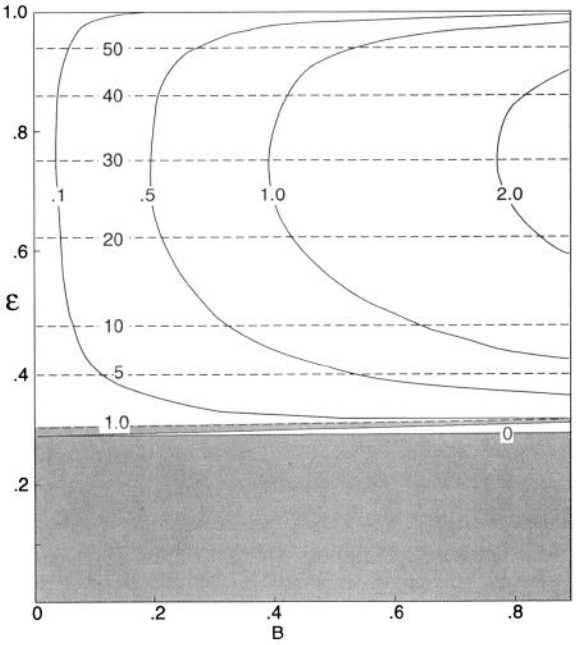

Figure 5. Same as Figure 4, but for $n = 10$ and $m = 60$.

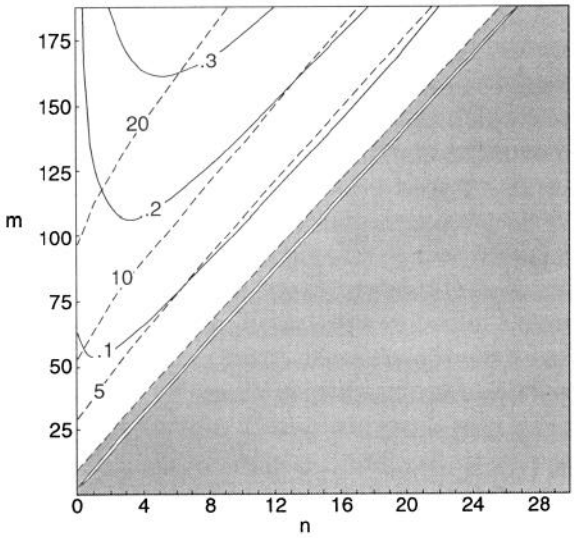

Figure 6. Contours of constant growthrate, $Im(\omega)$, (solid) and frequency, $Re(\omega)$, (dashed) in (n, m) space for $B = .1$ and $\epsilon = .25$. The shaded region is neutrally stable. At the top border between the shaded and unshaded regions $\omega = 1.0$. The region surrounded by shading is the subinertial region.

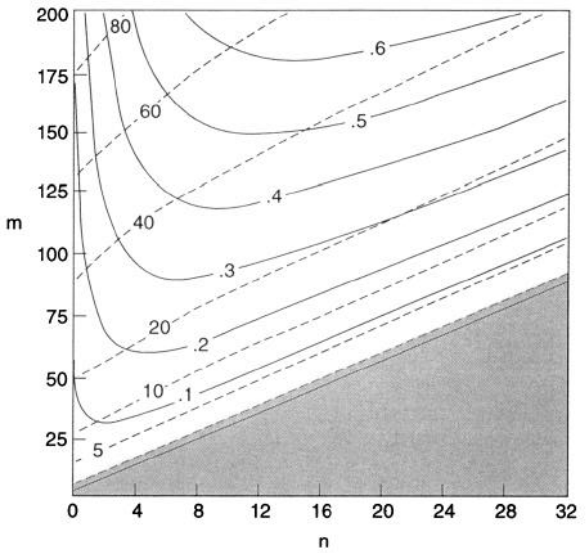

Figure 7. Same as Figure 6, but for $B = .1$ and $\epsilon = .5$. The line in the shaded region represents the subinertial region.

shown in Figures 7 and 9 which again shows the dominance of the superinertial waves.

For m, n and B fixed, the flow becomes more unstable for increasing ϵ until a maximum is reached as shown in Figures 4 and 5. However, for a fixed azimuthal

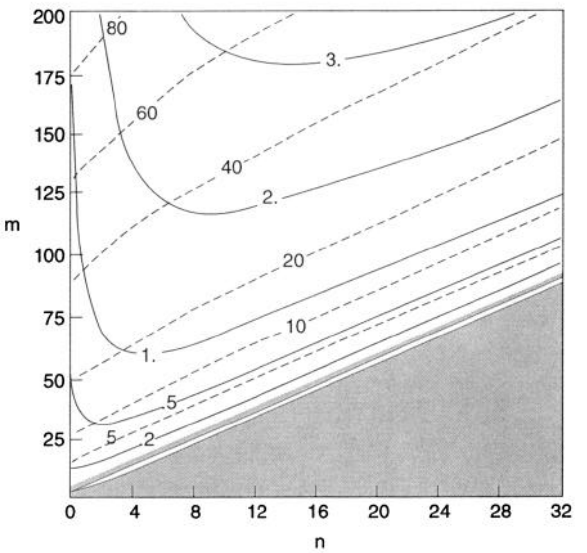

Figure 8. Same as Figure 6, but $B = .5$ and $\epsilon = .5$.

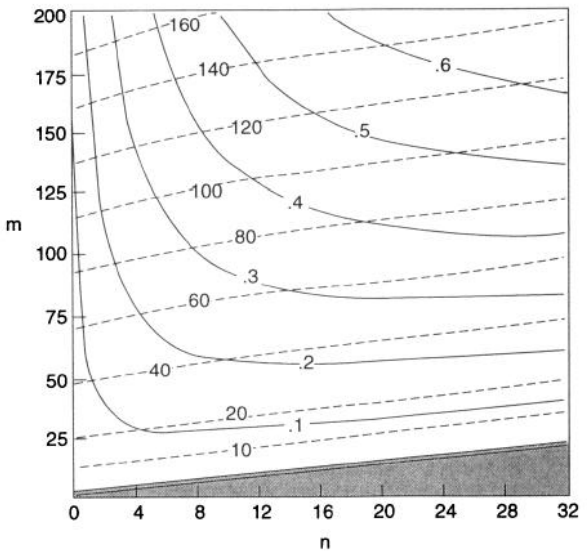

Figure 9. Same as Figure 6, but $B = .1$ and $\epsilon = .9$.

wavelength on the edge of the eddy (given nondimensionally by $2\pi/m\epsilon$) the flow becomes more stable with increasing ϵ. Thus in this sense the canonical front is more unstable than an eddy.

The internal wave radiation beneath the eddy from the unstable region for superinertial conditions will look very much like the straight rays in Figures 7 and 8 in (F). Theoretically those rays directed toward the central axis will turn away from the center on hyperbolic paths and never reach the center. In the real ocean, however, the bottom would almost always be encountered before the rays had a chance to curve very much.

We found in (F) that the maximum length scale, L, of the unstable region at the front is approximately given by $L = V_0/f$. This scale also applies fairly well to the edge of an eddy if the Rossby number, ϵ, is less than about 1/3 which would be true for almost all realistic eddies in the ocean. We note that L/r_0 is ϵ. So the Rossby number is a measure of the maximum fraction of the outer radius that can be unstable.

A more precise measure of the region of instability of our cylindrical geometry for $\epsilon > 1/3$ is the interval $|\gamma| < R < 1$, where the eigenfunctions of (23) are oscillatory. This interval at the edge of the eddy is greatest as $\epsilon \to 1$ when $|\gamma| = |m/\lambda|$ is minimum which occurs for $m = 1$ and $n = 0$, the values that are as small as possible but where instability is still possible. So from (37), assuming B is small, we have $|\lambda| \approx 1 + |m|$ and the maximum interval is $1/2 < R < 1$. Even for ϵ near one, this interval of instability squeezes down quickly as m and n increase as it does in (F).

We expect this unstable region to become turbulently mixed. But the intensity of mixing is not uniform over the region. The maximum value of the growthrate,

max $[Im(\omega)]$, is a measure of this intensity. For any ϵ, max $[Im(\omega)]$ increases from zero at $R = |\gamma|$ to infinity at $R = 1$. This variation can be approximately quantified using results from the analysis of the front. From (59) of (F), we can show that max $[Im(\omega)] \approx B/\pi(2n + 1)[(1/\sqrt{\bar{y}}) - 1]$ where the unstable region is $0 \leq \bar{y} \leq 1$ for $B \ll 1$. $\bar{y}$ is the dimensionless cross-front distance measured from the point where the front meets the surface and nondimensionalized by the length V_0/f where V_0 is the velocity at the front. This equation applies to the eddy for ϵ small if we let $\bar{y} \approx (1 - R)/\epsilon$. The dimensionless along the front wavenumber, k, will be $(2n + 1)/\bar{y}$ for the most unstable wave.

The most extensive observations of the edges of eddies are so-called 'meddies' which originate in the Mediterranean and are observed in the Atlantic. These eddies are generally not characterized by large density differences with their surroundings but by cores with higher salinity and temperature. Thus our model does not strictly apply. Armi *et al.* (1989) and Laanemets and Lips (1991), observing these kind of eddies in the Atlantic, note that lateral intrusion and mixing on the sides of the eddy are contributing most to its erosion. Ruddick (1992) has fairly well demonstrated that the mechanism of double diffusion dominates this intrusion. However, the instability described here should contribute to the initial breakdown of the interface, though the model would be difficult to apply after extensive double diffusion has occurred.

6. Summary and conclusions

For a realistic oceanic eddy ($\epsilon < 1/3$) the results from the investigation of the canonical front (Kroll (1992) = (F)) can be used to good approximation for the eddy. This can be done by replacing the dimensionless along the front wavenumber, k, in (F) by ϵm where ϵ is the Rossby number and m the angular mode number. Using those results and results found here, we conclude that:

(1) The eddy will be unstable in a boundary layer on the edge of the eddy which at a maximum cannot be any larger than one-half the radius. When ϵ is a realistic value for oceanic eddies ($<1/3$) the results of (F) apply and this maximum width is approximately V_0/f where V_0 is the velocity at the outer edge. This is equivalent to stating that this width will be a fraction ϵ of the radius.

(2) Since the instability for most realistic conditions is confined to the outer edge of the eddy ($O(10$ km) versus $O(100$ km)), the shape of the eddy near its edge is much more important than the overall shape of the entire eddy. Thus these results should apply to eddies not having a simple parabolic shape if the shape is approximately linear at the edge and the mean flow does not vary greatly there.

(3) The unstable region shrinks but becomes more unstable as m increases.

(4) For a given radial mode number, n, and Rossby number, ϵ, there is a minimum value of m which must be satisfied for instability, given by (38).

(5) The unstable wave is in the direction of the mean flow. From (F) we can show that the phase speed, ω/k, is always less than the mean flow speed.

(6) We have subinertial and superinertial regimes, but the superinertial will predominate.

(7) There will be rays of internal wave radiation originating from the unstable region of the eddy for frequencies greater than inertial. These rays will follow hyperbolas and can form caustics. Rays directed toward the center of the eddy turn before reaching the center.

We expect the unstable region to become turbulent and the sharp vertex of the velocity profile to round off. Thus the eddy should erode away at the edge even without friction. Since the time scale for the life of an oceanic eddy is $O(1\text{ yr.})$ (Armi *et al.,* 1989), a state of quasi-equilibrium would be expected to develop. This would suggest a future model using an eddy viscosity to represent the turbulent dissipation. Then we would like to know if this viscosity will stabilize the flow and, if so, to calculate how large this viscosity would have to be.

The method used here could also be applied to an inviscid model of a cold-core, cyclonic eddy which sits on the bottom. This problem would essentially be the upside down version of the one considered in this paper. However, since the eddy is at the bottom, friction would affect it much more than the surface affects a warm-core eddy. The edge of such a cold-core eddy, where our instability is located, would be at the bottom and the effect of bottom friction is unclear. An inviscid model may be too unrealistic. There are other regimes of cold-core eddy flows which would be interesting to investigate in a manner similar to this paper.

Acknowledgments. This work was supported by grant OCE-8915959 from the National Science Foundation.

REFERENCES

Armi, L., D. Hebert, N. Oakey, J. F. Price, P. L. Richardson, H. T. Rossby and B. Ruddick. 1989. Two years in the life of a Mediterranean salt lens. J. Phys. Oceanogr., *19,* 354–370.

Benjamin, T. B. 1963. The threefold classification of unstable disturbances. J. Fluid Mech., *16,* 436–443.

Cairns, R. A. 1979. The role of negative energy waves in some instabilities of parallel flows. J. Fluid Mech., *92,* 1–14.

Cushman-Roisin, B. 1986. Linear stability of large elliptical warm-core rings. J. Phys. Oceanogr., *16,* 1158–1164.

Cushman-Roisin, B., W. H. Heil and D. Nof. 1985. Oscillations and rotations of elliptical warm-core rings. J. Geophys. Res., *90,* 11756–11764.

Joyce, T. M. 1984. Velocity and hydrographic structure of a Gulf Stream warm-core ring. J. Phys. Oceanogr., *14,* 343–377.

Joyce, T. M., R. Backus, K. Baker, P. Blackwelder, O. Brown, T. Cowles, R. Evans, G. Fryxell, D. Mountain, D. Olson, D. Schlitz, R. Schmitt, P. Smith, R. Smith and P. Wiebe. 1984. Rapid evolution of a Gulf Stream warm-core ring. Nature, *308,* 837–840.

Kroll, J. 1982. An unstable uniform slab model of the mixed layer as a source of downward propagating near-enertial motion. Part 1: Steady mean flow. J. Mar. Res., *40,* 1013–1033.

—— 1988. Instability of a mixed layer model and the generation of near-inertial motion. Part I: Constant mixed layer depth. J. of Phys. Oceanogr., *18,* 963–976.

—— 1992. The stability of a canonical front. J. Mar. Res., *50,* 183–205.

Laanemets, J. J. and U. K. Lips. 1991. Fine structure of thermohaline fields in lenses of Mediterranean water. Oceanology, *31,* 135–139.

McWilliams, J. C. 1985. Submesoscale, coherent vortices in the ocean. Rev. of Geophys., *23,* 165–182.

Ostrovskiy, L. A. and L. Sh. Tsimring. 1981. Radiating instabilities of shear flows in a stratified fluid. Izv. Atmos. Oceanic Phys., *17,* 564–566.

Richardson, P. L. 1980. Gulf Stream ring trajectories. J. Phys. Oceanogr., *10,* 90–104.

Ripa, P. 1987. On the stability of elliptical vortex solutions of shallow-water equations. J. Fluid Mech., *183,* 343–363.

—— 1992. Instability of a solid-body rotating vortex in a two-layer model. J. Fluid Mech., *242,* 395–417.

Ruddick, B. 1992. Intrusive mixing in a Mediterranean salt lens—intrusion slopes and dynamical mechanisms. J. Phys. Oceanogr., *22,* 1274–1285.

Received: *10 September, 1992;* revised: *23 February, 1993.*